catalysts

MDPI

Article

The Influence of Cerium to Manganese Ratio and Preparation Method on the Activity of Ceria-Manganese Mixed Metal Oxide Catalysts for VOC Total Oxidation

Parag M. Shah, Liam A. Bailey and Stuart H. Taylor *

Cardiff Catalysis Institute, School of Chemistry, Cardiff University, Main Building, Park Place, Cardiff CF10 3AT, UK

* Correspondence: taylorsh@cardiff.ac.uk

Abstract: A set of ceria-manganese mixed metal oxide catalysts with varying Ce:Mn ratios were prepared by coprecipitation using sodium carbonate and were evaluated for the total oxidation of propane and naphthalene. Manganese-rich samples were the most active, with $Ce_{0.25}Mn_{0.75}O_x$ having the highest activity. Catalysts were characterised using X-ray diffraction, Brunauer-Emmett-Teller (BET) surface area, Raman spectroscopy, temperature programmed reduction (TPR), electron microscopy, and X-ray photoelectron spectroscopy (XPS), establishing that the high activity of $Ce_{0.25}Mn_{0.75}O_x$ was due to the formation of phase-separated Mn-substituted ceria and Mn_2O_3 phases that were not simultaneously present in the other catalysts. The catalyst preparation technique for the most active ratio was investigated using co-precipitation by urea, oxalic acid and citric acid, and mechanochemical grinding. For propane, the mechanochemical and urea catalysts were more active than the carbonate coprecipitated catalyst, due to greater surface area and increased phase separation. This work demonstrates that ceria-manganese mixed metal oxides are more active than the parent oxide, but that preparation technique is also important for controlling activity.

Keywords: ceria; manganese oxide; catalytic oxidation; VOC; propane; naphthalene

Citation: Shah, P.M.; Bailey, L.A.; Taylor, S.H. The Influence of Cerium to Manganese Ratio and Preparation Method on the Activity of Ceria-Manganese Mixed Metal Oxide Catalysts for VOC Total Oxidation. *Catalysts* **2023**, *13*, 114. https://doi.org/10.3390/catal13010114

Academic Editors: Fan Lin and Jong-Ki Jeon

Received: 1 December 2022
Revised: 21 December 2022
Accepted: 27 December 2022
Published: 4 January 2023

1. Introduction

Volatile Organic Compounds (VOCs) are common atmospheric organic pollutants, released from both natural and anthropogenic sources. They have extensive negative impacts on both the environment and human health. VOCs are typically powerful greenhouse gasses with global warming potentials significantly higher than carbon dioxide.[1] Others are potent carcinogens, with VOCs such as benzene and naphthalene being linked to instances of leukaemia [2]. They also readily react with NO_x to form ozone, a key constituent of photochemical smog and air pollution, especially in urban environments [3,4]. Air pollution is detrimental to human health and is the leading cause of preventable death worldwide [5]. This has led to the introduction of legislation that aims to reduce emissions of VOCs. The Gothenburg Protocol and China's 13th Five-Year Plan are all notable pieces of legislation that target lowering the concentration of VOCs in the atmosphere [6,7].

There are several methods that have been developed to help control the release of VOCs, these include thermal oxidation, absorption, adsorption, and catalytic oxidation [8,9]. Catalytic oxidation has undergone extensive research, due to its high selectivity, comparative low temperature of oxidation to thermal oxidation, and ability to treat low concentration streams [10]. Unlike absorption and adsorption, it is a destructive technique, rather than immobilising the VOCs. Thermal oxidation is also destructive, but compared to catalytic oxidation it has far greater potential to form highly toxic by-products and NO_X.

Investigations into the catalytic total oxidation of propane are numerous, due to the stability of propane compared to other VOCs [11]. Propane is one of the most challenging VOCs to oxidise, making it a good model reactant to assess the performance of catalysts. Emissions of propane have also increased in the past decade, due to increased use as a fuel in the form of liquified petroleum gas (LPG) [12]. Naphthalene is another widely researched VOC because it is the simplest poly-aromatic hydrocarbon (PAH), making it a good model reactant for other PAHs. It is highly carcinogenic and emitted from many combustion processes [13], so methods for controlling emissions are an important aim.

Initially, supported noble metal catalysts dominated research, with close to 75% of all catalysts studied for VOC oxidation belonging to this class [14]. However, high metal costs have driven an increase in research into cheaper metal oxide and mixed metal oxide catalysts [15]. Ceria is a well-studied material that is active for VOC oxidation. The facile redox cycle between Ce^{4+} and Ce^{3+}, along with high oxygen storage capacity and oxygen defect formation are beneficial characteristics for a total oxidation catalyst [16–19]. Ceria-based mixed metal oxides have been studied because they form the basis of highly active and stable catalysts for VOC oxidation. Previously, we have identified ceria-zirconia as a particularly active system for both propane and naphthalene oxidation, with synergy between the components leading to greater activity than the parent oxides [20,21]. Manganese oxides are also good VOC total oxidation catalysts, demonstrating high activity for naphthalene total oxidation [13]. This is due to easy cycling between Mn oxidation states, and high oxygen lability [22]. It has been found that Mn_2O_3 is more active than MnO_2 for naphthalene oxidation [23].

Ceria-manganese mixed metal oxide catalysts have been investigated for oxidation reactions. These mixed metal oxides have been shown to be highly active for the oxidation of CO, NO, ethanol, phenol, and toluene [24–33]. The ratio of Ce:Mn has an important influence over activity, with the smaller molecules preferring a more equal ratio of metals, while aromatics, were oxidised more readily by manganese-rich catalysts.

Preparation technique can have a large influence over the properties of a catalyst, and hence, their activity. Factors such as synthesis method, precursor, aging time, and heat treatment can all lead to differences in metal oxide catalyst characteristics. Preparation technique, cerium precursor and precipitating agent can all form a specific morphology of ceria with nanorods, nanowires, nanoplates or nanoparticles all being favoured by a particular method [17,34–38]. This will in turn impact factors such as surface area, reducibility, and oxygen storage capacity. Techniques such as mechanochemical grinding can also avoid the use of Na^+ or K^+ precursors which are known catalyst poisons, potentially leading to improved performance [20].

This work aims to investigate how the Ce:Mn ratio affects catalyst performance for the total oxidation of propane and naphthalene for catalysts prepared by coprecipitation using Na_2CO_3 precipitation. X-ray diffraction (XRD), Brunauer–Emmett–Teller (BET) surface area, Raman spectroscopy, temperature programmed reduction (TPR), scanning electron microscopy (SEM), and X-ray photoelectron spectroscopy (XPS) were all used to characterise the samples. The synthesis technique was also investigated to study how this effects catalyst performance for VOC oxidation and how it can modify catalyst morphology and characteristics.

2. Results and Discussion

2.1. Performance of Sodium Carbonate Coprecipitated Catalysts

An initial set of cerium manganese mixed metal oxide catalysts were prepared using sodium carbonate as the precipitating agent, and the focus was on the influence of cerium to manganese ratio on catalyst performance. The performance of the ceria-manganese mixed metal oxide catalysts for propane oxidation is shown in Figure 1. Minimal propane conversion occurred using a blank reactor tube (6% at 600 °C), suggesting that

homogeneous gas phase reactions for propane oxidation were negligible. All catalysts tested were highly selective for CO_2 formation (>99%), showing that total propane oxidation occurred.

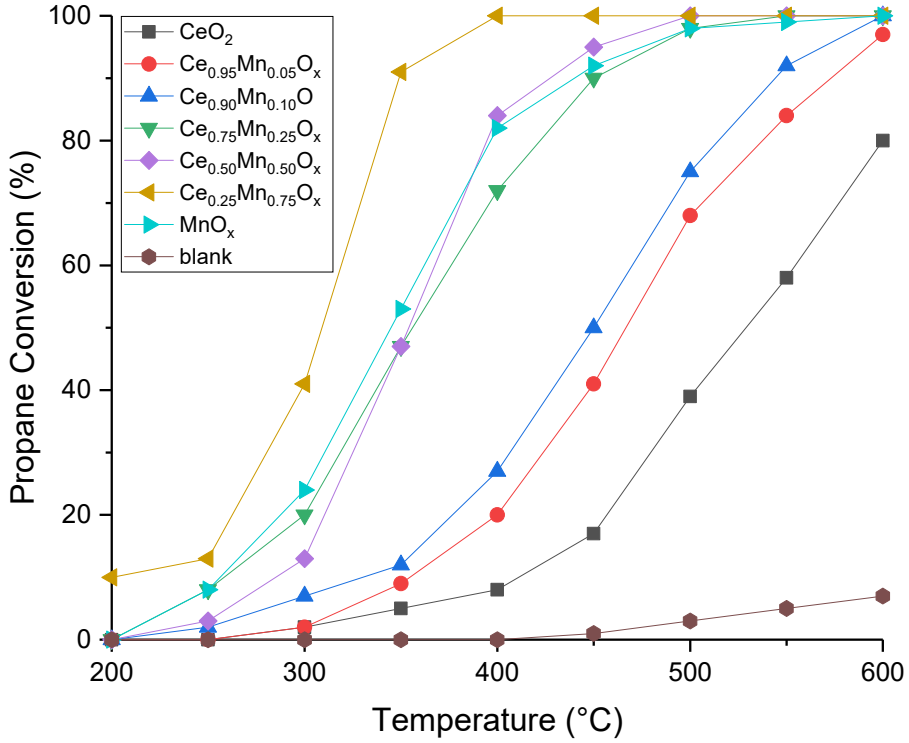

Figure 1. Propane conversion as a function of temperature for cerium-manganese mixed metal oxide catalysts prepared by sodium carbonate co-precipitation. Reaction conditions: 5000 ppm propane in air, Gas Hourly Space Velocity (GHSV) = 45,000 h^{-1}, Temperature range = 200–600 °C.

All ratios of the mixed metal oxides, along with the pure manganese oxide catalyst, were more active than the ceria catalyst, which did not fully convert the propane over the temperature range studied. A similar observation was made by Ren et al. [39] as at 600 °C, only 80% propane conversion was achieved. The activity for the manganese oxide was higher than the ceria, with full conversion of propane achieved by 500 °C, this agrees with work in the literature where MnO_x was more active than CeO_2 for the total oxidation of VOCs such as ethanol, ethyl acetate, toluene, and propane [29,39].

The addition of manganese to ceria led to an increase in activity in all instances. All the manganese-rich mixed metal oxides performed particularly well when compared to the catalysts that contained more ceria. The $Ce_{0.25}Mn_{0.75}O_x$ catalyst was the most active catalyst in terms of propane oxidation, with the $Ce_{0.5}Mn_{0.5}O_x$, MnO_x, and $Ce_{0.75}Mn_{0.25}O_x$ catalysts all having similar performance. This was particularly notable at low temperature where the T_{20} and T_{50} were 35 °C and 40 °C lower for the $Ce_{0.25}Mn_{0.75}O_x$ than the next best catalyst. The following performance trend was established for the range of catalysts:

$Ce_{0.25}Mn_{0.75}O_x$ > $Ce_{0.5}Mn_{0.5}O_x$ ~ MnO_x ~ $Ce_{0.75}Mn_{0.25}O_x$ > $Ce_{0.9}Mn_{0.1}O_x$ > $Ce_{0.95}Mn_{0.05}O_x$ > CeO_2

The performance of the catalysts for the total oxidation of naphthalene is presented in Figure 2. All catalysts were active and a blank reaction was performed showing negligible naphthalene conversion in an empty tube at all temperatures, suggesting gas phase homogeneous reactions were not contributing to naphthalene conversion. As with the propane tests, ceria was the least active catalyst with a CO_2 yield of just 35% at 250 °C. The MnO_x, $Ce_{0.25}Mn_{0.75}O_x$, $Ce_{0.5}Mn_{0.5}O_x$, and $Ce_{0.75}Mn_{0.25}O_x$ all reached 100% CO_2 yield at 200 °C; however, the manganese-rich samples were all significantly more active at low temperature. Large changes in activity were apparent between temperature increments where CO_2

yield can increase from low values (around 10–20%) to a high yield. This is characteristic of studies into naphthalene oxidation and has been seen in previous studies [20,21]. Again, the $Ce_{0.25}Mn_{0.75}O_x$ was the most active catalyst. The activity trend for these catalysts for total naphthalene oxidation are as follows:

$Ce_{0.25}Mn_{0.75}O_x$ > MnO_x > $Ce_{0.5}Mn_{0.5}O_x$ > $Ce_{0.75}Mn_{0.25}O_x$ > $Ce_{0.9}Mn_{0.1}O_x$ > $Ce_{0.95}Mn_{0.05}O_x$ > CeO_2.

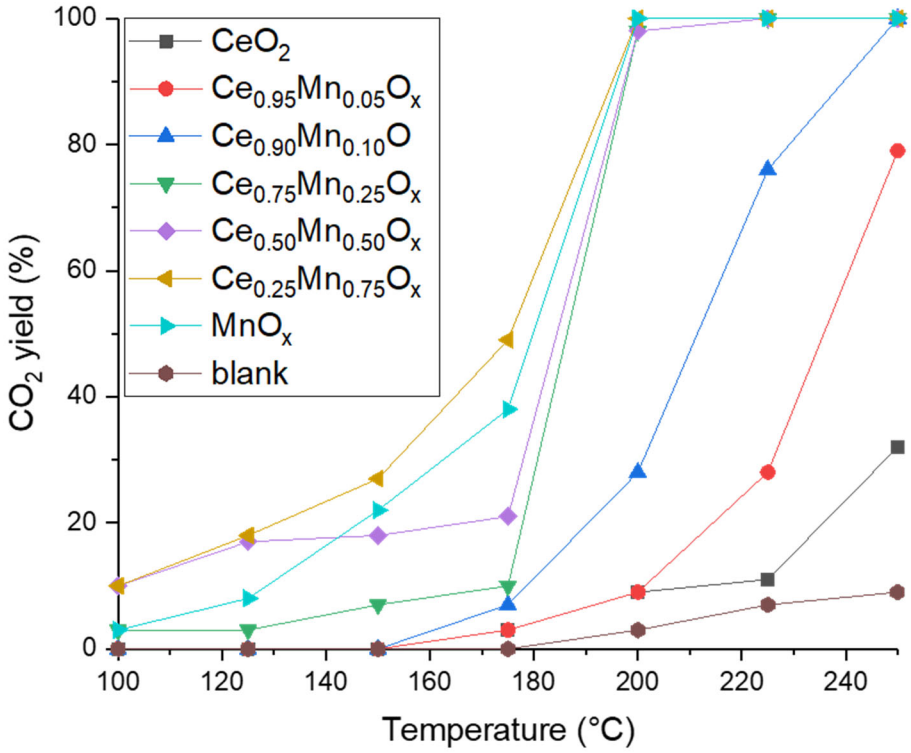

Figure 2. CO_2 yield as a function of temperature studying the total oxidation of naphthalene for cerium-manganese mixed metal oxide catalysts prepared by sodium carbonate co-precipitation. Reaction conditions: 100 ppm naphthalene/20% O_2/He, Gas Hourly Space Velocity (GHSV) = 45,000 h^{-1}, Temperature range = 100–250 °C.

2.2. Characterisation of Sodium Carbonate Coprecipitated Catalysts

Powder X-ray diffraction (XRD) was performed on the catalysts, with the diffraction patterns and derived data shown in Figure 3 and Table 1. Ceria prepared by precipitation had four major peaks around 28°, 33°, 49°, and 57° corresponding to the (111), (200), (220), and (311) lattice planes of cubic fluorite phase ceria. Analysis of the manganese oxide catalyst suggests a mixture of phases was present. Peaks around 29°, 39°, 57°, and 74° are all indicative of MnO_2 [40]; whilst peaks around 32°, 37°, 44°, and 52° all correspond to Mn_2O_3 [41]. The relative intensities of the peaks suggest the material is largely Mn_2O_3 with MnO_2 a lesser component.

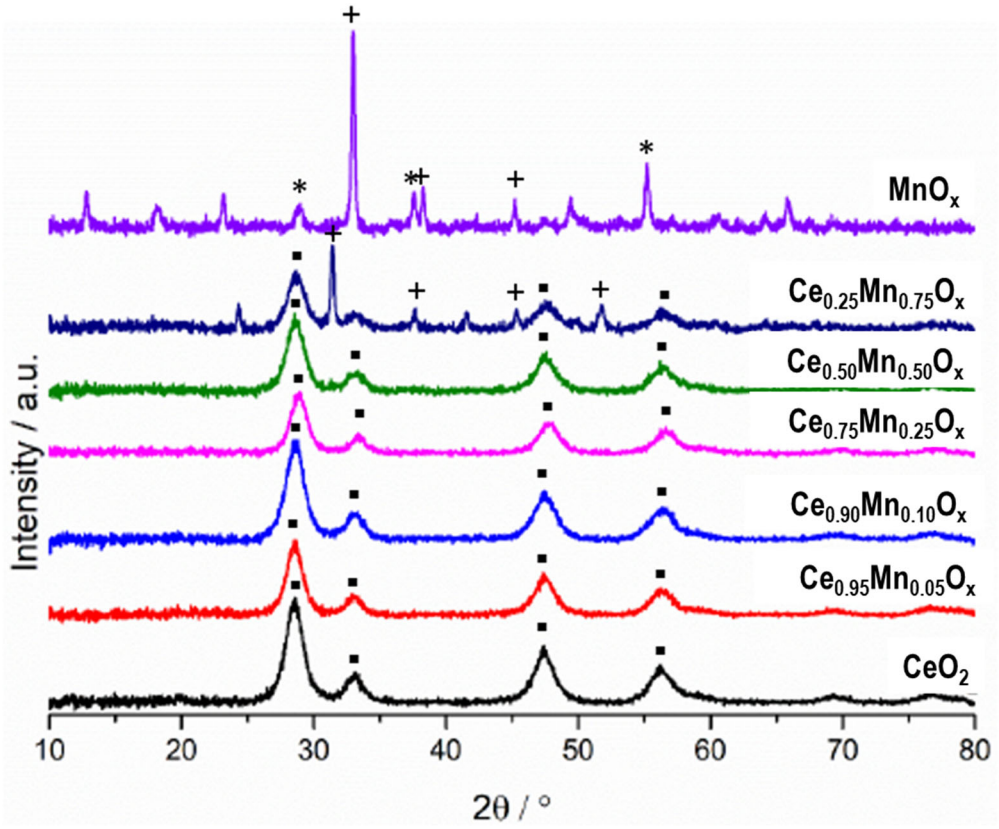

Figure 3. Powder XRD patterns of sodium carbonate co-precipitated cerium-manganese mixed metal oxide catalysts. ▪—ceria phases, *—MnO_2 phases, +—Mn_2O_3 phases.

Table 1. Physiochemical properties extracted from XRD of cerium-manganese mixed metal oxide catalysts.

Sample	Phases Present	Position of CeO_2 (111) Reflection (°)	Average Crystallite Size (Å)		D-Spacing from (200) Lattice Plane (Å)	Unit Cell Volume (Å)
			CeO_2	MnO_x		
CeO_2	**CeO_2**	**28.6**	**106**	-	2.74	164.6
$Ce_{0.95}Mn_{0.05}O_x$	CeO_2	28.7	47	-	2.72	161.0
$Ce_{0.9}Mn_{0.1}O_x$	CeO_2	28.7	43	-	2.71	159.2
$Ce_{0.75}Mn_{0.25}O_x$	CeO_2	29.0	63	-	2.70	157.5
$Ce_{0.5}Mn_{0.5}O_x$	CeO_2	28.8	60	-	2.68	154.0
$Ce_{0.25}Mn_{0.75}O_x$	CeO_2/Mn_2O_3	28.8	41	152	2.69	155.7
MnO_x	MnO_2/Mn_2O_3	-		361		

The XRD patterns for all the mixed metal oxide samples also showed peaks for cubic ceria. The intensity of the ceria peaks decreased as the amount of manganese in the mixed metal oxide increased, and the position of the ceria (111) peak shifted to a higher angle. This suggests the formation of a mixed cerium-manganese oxide phase in the catalyst, with the manganese incorporated into the ceria lattice. This shift to a higher Bragg angle has been seen in other ceria-based mixed metal oxides to suggest incorporation [20,26,30]. The $Ce_{0.25}Mn_{0.75}O_x$ catalyst has shifted cubic ceria peaks, along with peaks around 32°, 37°, and 52°, corresponding to bulk Mn_2O_3. This demonstrates the formation of phase separated ceria incorporated manganese and Mn_2O_3 oxides. This suggests that for all the mixed metal oxide catalysts except $Ce_{0.25}Mn_{0.75}O_x$, the manganese has solely incorporated into the ceria lattice, whilst the $Ce_{0.25}Mn_{0.75}O_x$ also has discrete Mn_2O_3. Bulk Mn_2O_3 has been reported as a highly active phase for VOC oxidation so the increased presence of this phase in the $Ce_{0.25}Mn_{0.75}O_x$ catalyst can help explain the higher activity seen for propane and naphthalene oxidation, when compared to the other mixed metal oxides studied [23].

The (200) cubic ceria peak has been used to calculate the d-spacing and unit cell volume (Table 1). As the manganese concentration increased, the d-spacing decreased, providing evidence for the incorporation of the manganese into the ceria lattice. Manganese incorporation was maximised for the $Ce_{0.25}Mn_{0.75}O_x$ catalyst. Manganese has a smaller ionic radius than cerium, so substitution into the ceria lattice causes a contraction of lattice parameter.

The addition of manganese into the cerium lattice also results in a decrease in the average crystallite size of the CeO_2 phases when compared to pure CeO_2. This has been observed in previous studies of ceria-manganese mixed metal oxides and provides evidence for manganese incorporation [26,30,42]. It was found that the presence of manganese inhibits ceria crystallite growth and can help explain the lower crystallite size seen for the mixed metal oxide when compared to the bulk CeO_2 [24].

Surface area was measured using the BET method and the formation of a mixed metal oxide led to higher surface area when compared to just the parent metal oxide (Table 2). Surface area increased as the proportion of manganese increased, with the $Ce_{0.25}Mn_{0.75}O_x$ sample having the largest surface area, and this could be an important parameter for catalyst performance. For the mixed metal oxides, when rate of reaction is normalised to the surface area (Table S1), the rate does increase as surface area increases. However, there is no clear relationship between these variables suggesting that other factors are more important in determining activity.

Table 2. Brunauer-Emmett-Teller (BET) Surface area and Raman characteristics of sodium carbonate co-precipitated ceria-manganese mixed metal oxide catalysts. FWHM = full width half maximum.

Catalyst	BET Surface Area ($m^2\ g^{-1}$)	Raman FWHM of 464 cm^{-1} peak (cm^{-1})	Peak Area Ratio of 600 cm^{-1}/464 cm^{-1}
CeO_2	21	38.4	0.0627
$Ce_{0.95}Mn_{0.05}O_x$	29	48.3	0.0671
$Ce_{0.9}Mn_{0.1}O_x$	29	50.3	0.0996
$Ce_{0.75}Mn_{0.25}O_x$	34	81.2	0.5408
$Ce_{0.5}Mn_{0.25}O_x$	39	-	-
$Ce_{0.25}Mn_{0.75}O_x$	41	-	-
MnO_x	18	-	-

Raman spectroscopy was performed on the catalysts (spectra in Figure S1 and summarised in Table 2). The spectra for the pure ceria sample supported the XRD conclusion for the formation of cubic fluorite ceria, whilst also showing the presence of Frenkel-type oxygen vacancies. The same peaks were also seen in the mixed metal oxide catalysts, again confirming the formation of a cubic ceria-based phase, although substituted. The intensity of these peaks decreased as the proportion of ceria in the mixed metal oxide decreases, whilst the full width half maximum (FWHM) of the 464 cm^{-1} peak increased. This characteristic has been linked to a decrease in particle size and an increase in the number of defect sites and oxygen vacancies, which have been found to increase activity in ceria-based catalysts for VOC oxidation [43]. An increase in these sites can help explain why the manganese-rich catalysts tested here are more active. Oxygen vacancies are created by the substitution of manganese into the ceria lattice and can also be monitored by the peak at 600 cm^{-1} which corresponds to the Frenkel-type oxygen vacancies. Comparing the peak area ratio of this peak to the 464 cm^{-1} peak suggests a large increase in defects as more manganese was incorporated. This can help explain the better performance of the catalysts, and the same conclusion has been observed in previous studies for toluene oxidation using ceria-based catalysts [44].

Reduction profiles obtained from temperature-programmed reduction (Figure 4) show a number of different oxidation states present in the mixed metal oxide catalysts. There has generally been a shift to lower temperature of the peak corresponding to surface

ceria when manganese was present compared to the pure ceria sample. This suggests that the addition of manganese led to the catalysts becoming more easily reducible, with previous work suggesting this is caused by the incorporation of the manganese into the ceria lattice [25]. The area of this peak also increased as manganese content increased, due to the increasing surface areas of these samples. Hence, more easily reducible species are present at the surface that are more active in redox cycles and influence catalysis.

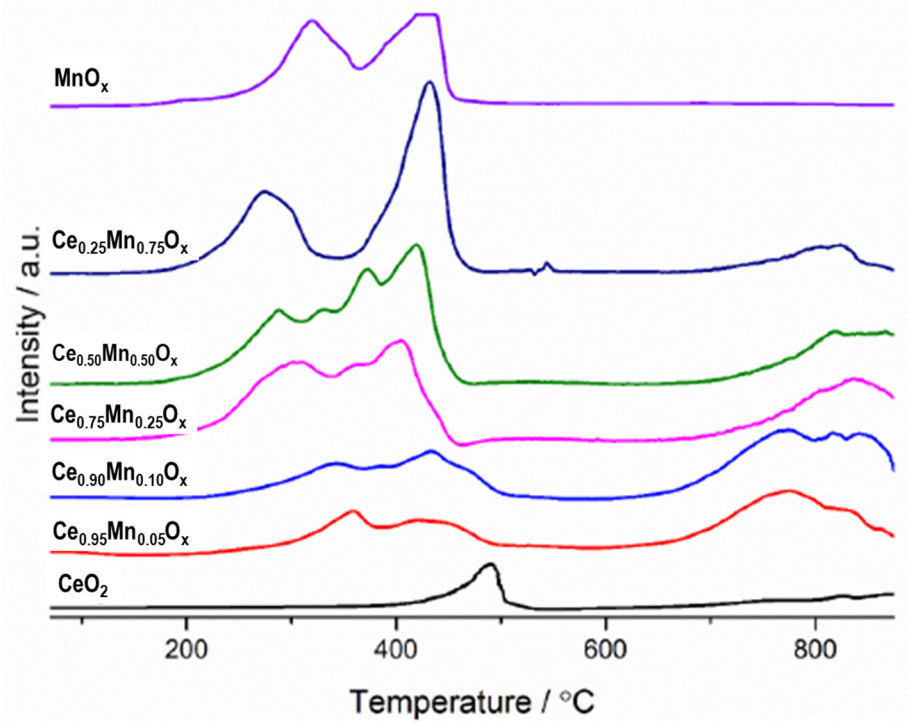

Figure 4. H_2 temperature programmed reduction (TPR) profiles of ceria-manganese catalysts synthesised by co-precipitation using sodium carbonate. Reaction conditions: 30 mL min^{-1} 10% H_2/Ar, Temperature range = 50–850 °C.

The mixed metal oxides have very different surface reduction profiles. The $Ce_{0.95}Mn_{0.05}O_x$ and $Ce_{0.9}Mn_{0.1}O_x$ both have two peaks, corresponding to reduction in surface ceria and lattice ceria. This double peak has been seen in other ceria-manganese mixed metal oxides [45]. The complex shape of this peak also suggests contribution of manganese phases to the reduction profile of these catalysts. As no manganese phases were identified by XRD it would suggest large amounts of incorporation of the manganese into the ceria lattice. The $Ce_{0.75}Mn_{0.25}O_x$ and $Ce_{0.5}Mn_{0.5}O_x$ have three and four peaks, respectively, suggesting the catalyst surface may contain a complex mix of reducible species, with phases that may not be detectable by XRD. The profile for $Ce_{0.25}Mn_{0.75}O_x$ had two peaks corresponding to a reduction in Mn_2O_3 to Mn_3O_4 and the reduction in surface ceria. This shows good agreement with the XRD pattern as it suggests the presence of discrete areas of both manganese-substituted ceria and Mn_2O_3. The broad peaks present for the mixed metal oxide catalysts at 800 °C show that the manganese is having a significant effect on the reducibility of bulk ceria. This has been seen in previous studies into ceria manganese materials and was thought to increase lattice defects and improve oxygen lability [27,45]. These are all characteristics that have been shown to improve activity for VOC oxidation.

Scanning electron microscopy was performed on the catalysts, the pure ceria having a plate-like morphology, whilst the manganese oxide sample consists of smaller crystallites layered on top of each other (Figure S2i). The images for the mixed metal oxide catalysts show that the ceria plate-like morphology was retained; however, as the manganese content was increased, bulbous deposits formed on the platelets (Figure S2ii). The

$Ce_{0.25}Mn_{0.75}O_x$ sample showed distinct plate-like and bulbous areas, providing further evidence of some phase separation of ceria and manganese oxide phases that was suggested by the XRD (Figure 3). Energy-dispersive X-ray spectroscopy (EDX) analysis (Figure S3) was also performed with the elemental maps produced showing generally good mixing of the ceria and manganese in the ceria rich samples, in good agreement with previous characterisation described. However, the EDX does suggest that some phase separation has occurred for the $Ce_{0.5}Mn_{0.5}O_x$ sample as there are areas that are rich in either cerium or manganese. This could help explain why $Ce_{0.5}Mn_{0.5}O_x$ is more active than the ceria-rich catalysts, as there was the presence of discrete areas of active manganese oxide. This phase separation was also seen for the $Ce_{0.25}Mn_{0.75}O_x$ sample confirming characteristics measured by XRD and TPR.

The EDX also shows large amounts of sodium being present, despite washing performed during the synthesis. Surface sodium has been shown to be detrimental to catalyst activity for oxidation reactions on both ceria and manganese oxide-based catalysts [46,47], suggesting that preparation techniques using sodium-containing precipitating agents may not be optimal for catalysts synthesized with the intention of VOC oxidation reactions. Material synthesis techniques that forgo sodium precursor should be considered.

The Ce 3d XPS spectra exhibited peaks at 917 eV, an unsymmetrical doublet at 879 eV and 897 eV which are characteristic of Ce^{4+}, and a symmetrical doublet at 881 and 900 eV which indicates the presence of Ce^{3+} (Figure 5). The peak at 917 eV was very intense in all samples, indicating large amounts of Ce^{4+} present in all samples. The doublet peak between 903–895 eV became more symmetrical as the amount of manganese increased. This suggests an increase in the surface concentration of Ce^{3+} as the concentration of manganese increased. This again indicates the generation of a greater number of defect sites and oxygen vacancies caused by the manganese incorporation into the ceria lattice, which has been shown to help improve catalyst activity.

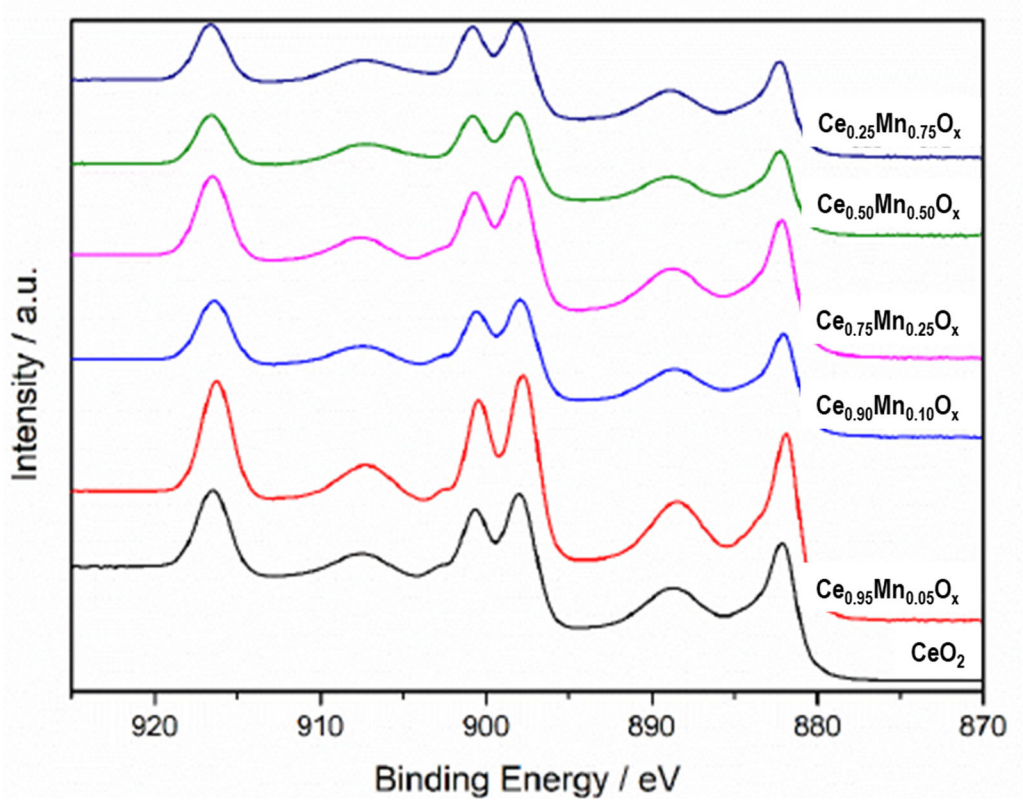

Figure 5. Ce 3d XPS spectra for the ceria-manganese samples prepared by sodium carbonate co-precipitation.

The peak splitting of the Mn 3s spectra can be used to determine the oxidation state of the manganese [48], this can be seen in Figure 6. All of the manganese-containing compounds, except the $Ce_{0.25}Mn_{0.75}O_x$, had a splitting of <5.3 eV, which is indicative of manganese in a 4+ oxidation state and mainly exists as the MnO_2 phase. The $Ce_{0.25}Mn_{0.75}O_x$ sample has a peak splitting of 5.5 eV, which suggests the manganese oxide present at the surface is Mn_2O_3. As previously stated, this phase of manganese oxide has been found to be the most active for VOC oxidation so can explain why the $Ce_{0.25}Mn_{0.75}O_x$ mixed metal oxide is the most active.

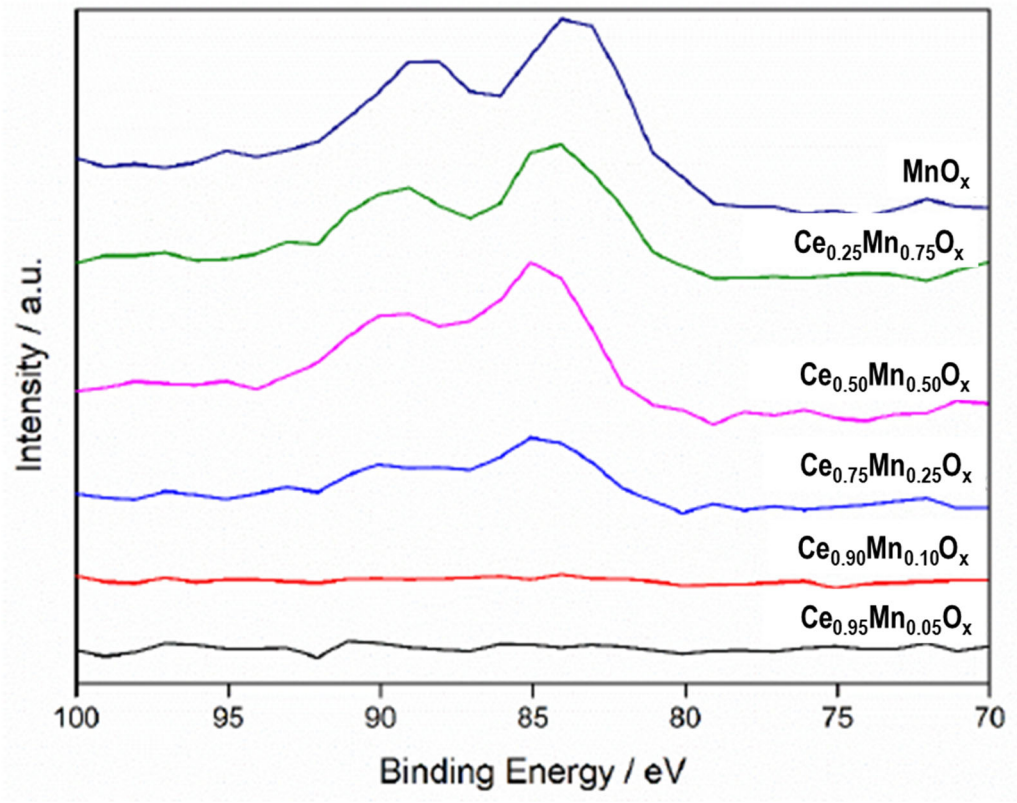

Figure 6. Mn 3s XPS spectra for ceria-manganese mixed metal oxide catalysts prepared by co-precipitation with sodium carbonate.

The XPS data were also used to calculate the concentrations of the species at the surface (Table S2). By comparing the relative ratio of cerium to manganese, good agreement was seen between the theoretical values for each component and what is seen at the surface. The XPS is also consistent with the EDX analysis, in that there are large amounts of sodium present on the surface of the catalysts. The concentrations of sodium are significantly higher from the XPS suggesting that the sodium is present mainly at the surface as opposed to mixed throughout the bulk. This surface sodium could block access to the catalyst active sites leading to reduced amounts of VOC oxidation, meaning a different synthesis technique that does not involve sodium-based precursors could potentially produce more active catalysts.

2.3. Influence of Preparation Method

To test the hypothesis around the detrimental effect of sodium, the most active $Ce_{0.25}Mn_{0.75}O_x$ catalyst was synthesised using several different techniques that did not involve a sodium precursor. The preparation technique of ceria-manganese mixed metal oxides has also been shown in the past to exert a significant influence over catalyst activity, especially for aromatic VOC oxidation [49,50]. The preparation methods investigated

were coprecipitation with urea, oxalic acid, and citric acid, and mechanochemical grinding of either carbonates or nitrates in a planetary ball mill.

The activity for propane oxidation is shown in Figure 7. Both catalysts prepared using urea and mechanochemically using carbonates were significantly more active than the Na_2CO_3 coprecipitation method. At 300 °C both these newly synthesised catalysts had 60% propane conversion, compared to the 40% for the Na_2CO_3 precipitated catalyst. This culminates in full conversion being achieved by 350 °C for the mechanochemical carbonate and urea methods, 50 °C lower in temperature than the Na_2CO_3 method. The catalyst prepared in a ball mill using a nitrate precursor exhibited very similar activity to the Na_2CO_3 catalyst. Conversely, the sample made using citric acid and oxalic acid had significantly lower activity than all of the other $Ce_{0.25}Mn_{0.75}O_x$ catalysts tested only reaching full conversion at 500 °C.

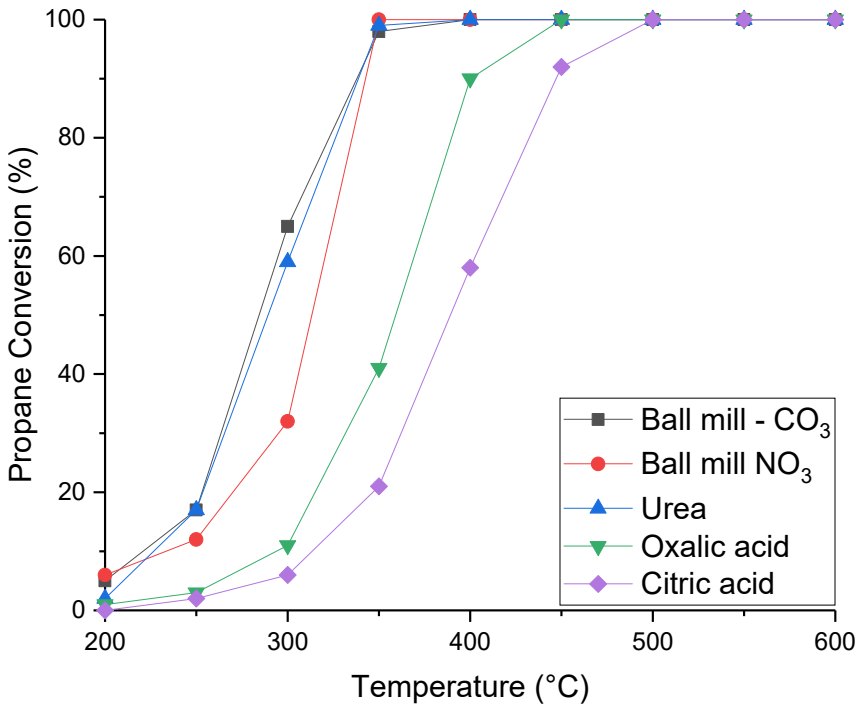

Figure 7. Propane conversion as a function of temperature of $Ce_{0.25}Mn_{0.75}O_x$ catalysts synthesised by different methods. Reaction conditions: 5000 ppm propane in air, Gas hourly space velocity (GHSV) = 45,000 h^{-1}, Temperature = 200–600 °C.

The catalysts were also tested for naphthalene total oxidation, with very different trends observed (Figure 8). All of the sodium-free catalysts were significantly less active than the $Ce_{0.25}Mn_{0.75}O_x$ catalyst made using sodium carbonate. Very little activity was seen for both the oxalic acid, citric acid and urea prepared catalysts. Whilst the mechanochemically prepared catalysts did reach 100% CO_2 yield, this occurred at a higher temperature than the Na_2CO_3 sample. Very little activity was recorded until 220 °C, where 40% CO_2 yield was achieved, whilst at the same temperature the Na_2CO_3 sample had 100% conversion to CO_2. It can be noted that for the materials made using Na_2CO_3, the catalysts generally follow the same activity trend for propane and naphthalene oxidation where an active catalyst for propane oxidation is also active for naphthalene oxidation. This has also been seen in other studies investigating the activity of mixed metal oxides for both these reactions [20,21]. However, this is not the case with catalysts synthesized using different preparation methods. For example, the catalyst prepared using urea was active for propane oxidation but performed poorly for naphthalene oxidation. There has been limited investigation into the role of different mixed metal oxides and synthesis technique so general trends between both reactions cannot be drawn.

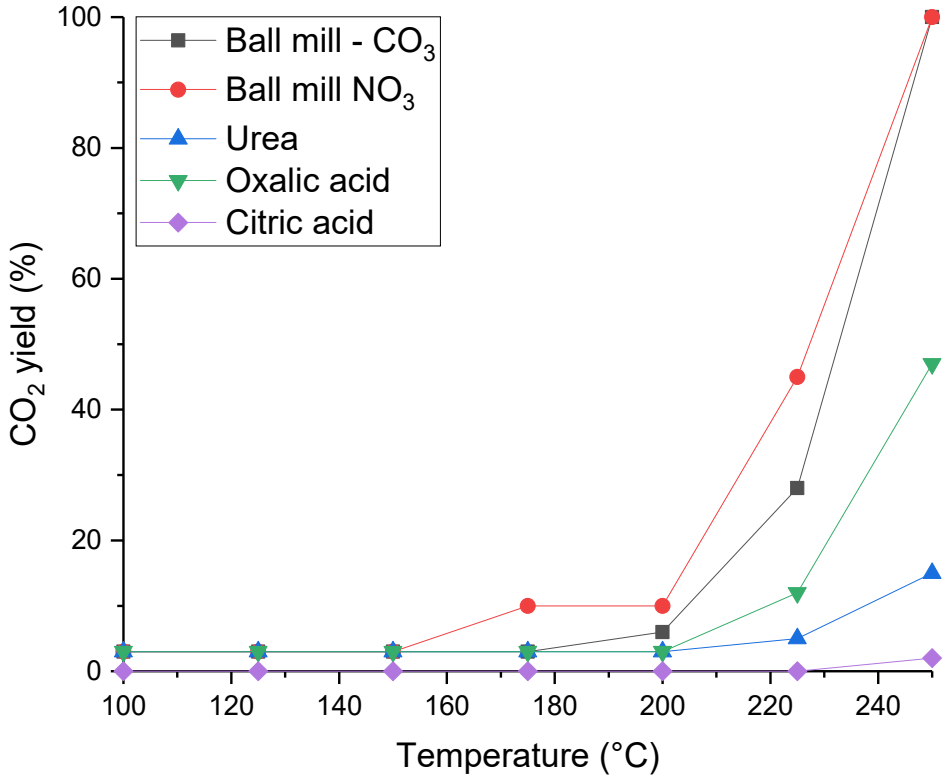

Figure 8. CO_2 yield as a function of temperature for the total oxidation of naphthalene for $Ce_{0.25}Mn_{0.75}O_x$ prepared by different synthesis techniques. Reaction conditions: 100 ppm naphthalene/20% O_2/He, GHSV = 45,000 h^{-1}, Temperature range = 100–250 °C.

The XRD patterns for the catalysts are presented in Figure 9. There is very little similarity in the diffraction patterns, showing that preparation technique had a large impact on sample crystallinity and the phases present. The oxalic acid sample appears much more amorphous than the other catalysts, with only one significant crystalline phase corresponding to Mn_2O_3. The citric acid prepared sample only had reflections for cubic fluorite ceria possibly suggesting that most of the manganese had been incorporated into the ceria lattice. A shift to a higher Bragg angle for the CeO_2 (111) peak and a contraction in the unit cell volume (Table 3) support this being the case. Both the urea and mechanochemically prepared samples had a mixture of phase separated ceria and manganese oxide reflections, with both containing cubic fluorite ceria, but while the urea and nitrate-precursor mechanochemically ground samples had MnO_2, the manganese phase for the carbonate precursor mechanochemical sample was Mn_2O_3. This can help explain the superior performance of the ball milled carbonate catalyst as it contained manganese in its more active oxide form. The ceria (111) peak for the mechanochemically prepared catalysts was also at the lowest angle suggesting very little incorporation of the manganese into the ceria lattice, and instead large amounts of phase separation between the two metal oxides. This value was also lower than seen in the Na_2CO_3 precipitated catalyst suggesting ball milling could encourage separation of the metal oxide phases, helping to explain the increased activity for propane oxidation.

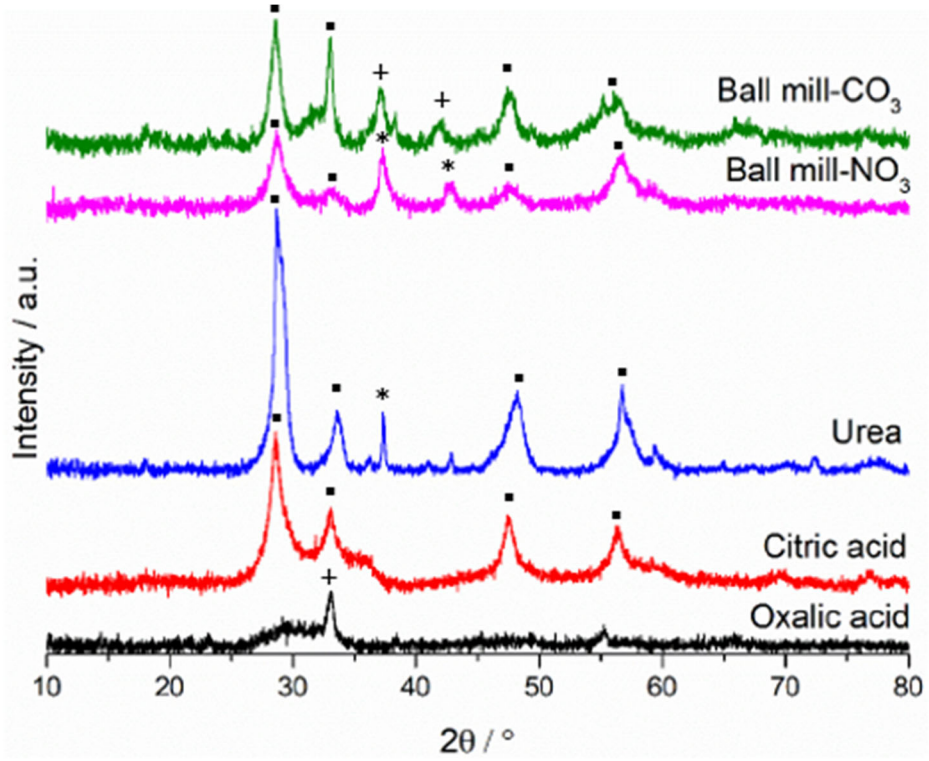

Figure 9. Powder XRD scattering patterns of $Ce_{0.25}Mn_{0.75}O_x$ catalysts. ▪—ceria phases, *—MnO_2 phases, +—Mn_2O_3 phases.

Table 3. Physical properties of $Ce_{0.25}Mn_{0.75}O_x$ catalysts.

Sample	Phases Present	Position of CeO_2 (111) Reflection (°)	Average Crystallite Size (Å)		Unit Cell Volume (Å³)	BET Surface Area ($m^2 g^{-1}$)
			CeO_2	MnO_x		
Mechanochemical grinding–carbonates	CeO_2 Mn_2O_3	28.4	156	216	168.20	83
Mechanochemical grinding–nitrates	CeO_2 MnO_2	28.8	63	111	157.46	44
Urea co-precipitation	CeO_2 Mn_2O_3	28.8	75	68	152.27	59
Oxalic acid	Mn_2O_3	-	-	51	-	53
Citric acid co-precipitation	CeO_2	28.7	101	89	157.46	3

Large differences of BET surface area were obtained depending on the preparation technique (Table 3). The mechanochemically prepared carbonate catalyst had the highest area, followed by the urea and oxalic acid precipitated catalyst and material prepared using nitrate precursors. Both these catalysts had surface areas and activity for propane oxidation higher than the sodium-precipitated catalyst. The citric acid synthesised catalyst had the lowest surface area of all the preparation techniques and the lowest activity for both propane and naphthalene oxidation of all $Ce_{0.25}Mn_{0.75}O_x$ catalysts tested. When the rate is normalised to surface area (Table S3) no correlation can be seen between surface area and catalyst performance suggesting other characteristics are responsible for activity.

Reduction profiles (Figure 10) were also recorded for these catalysts, showing that the preparation technique has a large effect on the reducibility of the catalyst. The mechanochemical carbonate catalyst had reduction peaks at 290 °C and 400 °C, which are

characteristic of Mn_2O_3 [51], corresponding well with the XRD analysis. The reduction peak for bulk ceria at 700 °C was lower than typically expected for this reduction, suggesting that manganese had also incorporated into the bulk ceria. The urea sample displayed 3 low intensity peaks (300 °C, 400 °C and 475 °C). The peaks at 300 °C and 475 °C correspond to bulk MnO_2 being phase separated from the ceria. The peak at 400 °C relates to the reduction in surface ceria. The phase separation can help explain the high activity of these samples as they both have bulk manganese oxide present, which is more active than bulk ceria, presumably the presence of ceria helps to disperse the more active manganese oxide and modifies redox behaviour to create the highly active catalyst. The citric acid and oxalic acid both had two peaks, which corresponds to bulk Mn_2O_3 and surface ceria. This suggests that some phase separation has occurred between the two phases; however, as the Mn_2O_3 does not appear in the XRD, it suggests it is either amorphous in nature, present with very small crystallites, or may only be present at low concentrations. The bulk ceria reduction peak lowered to 700 °C, again suggests the presence of manganese-substituted bulk ceria. The nitrate precursor ball mill-prepared sample only had one large reduction peak corresponding to MnO_2.

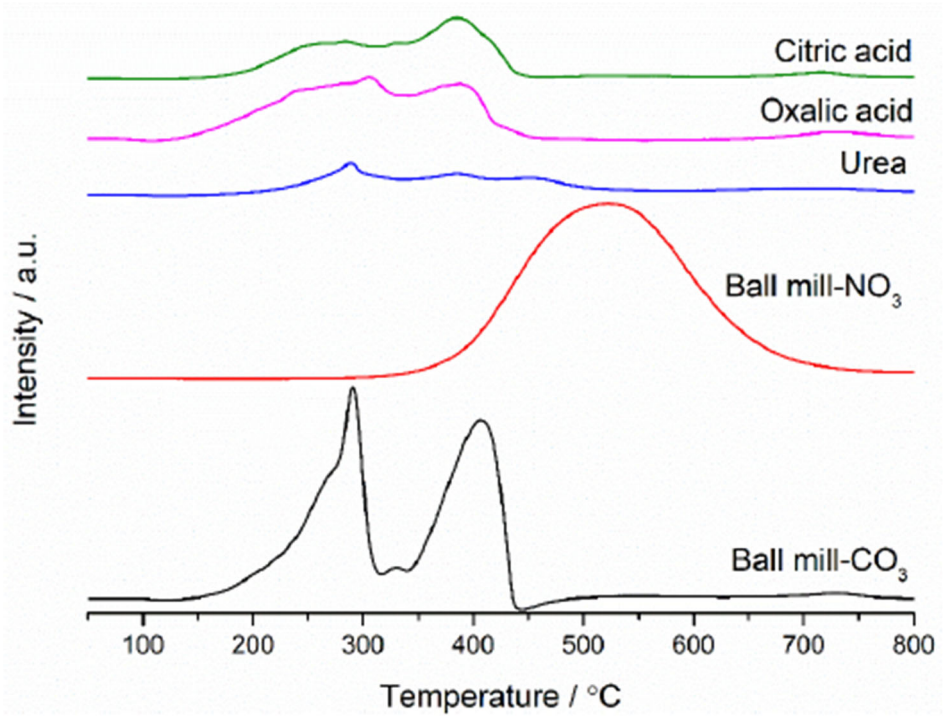

Figure 10. TPR profiles of $Ce_{0.25}Mn_{0.75}O_x$ sample. Reaction conditions: 10% H_2/Ar 30 mL min^{-1}, Temperature range 50–800 °C.

SEM images (Figure S4) highlight how much of an effect the preparation technique has on the morphology of the mixed metal oxides. The citric acid preparation formed a smooth net-like structure with large pores. This suggests the formation of a very ceria-like bulk structure as ceria prepared by this method has been observed previously [52,53]. This agrees with the XRD, which only showed the presence of crystalline CeO_2 phases. However, EDX imaging does show high levels of dispersed manganese suggesting that it has incorporated into the lattice (Figure S5). Similar to the Na_2CO_3 prepared sample, the urea method resulted in the formation of bulbous structures; however, this appeared to form on rod-like morphologies as opposed to platelets. The mechanochemically synthesised materials produced platelet-like structures while the oxalic acid prepared sample had a folded plate-like structure. EDX analysis performed with the SEM imaging showed large levels of mixing of the cerium and manganese throughout all catalysts, excluding the carbonate mechanochemical one, suggesting high amounts of intimate incorporation of the

manganese. The carbonate mechanochemical catalyst instead displayed areas that were manganese rich with low concentrations of ceria. This again provides evidence that the ball milling of carbonates gives high levels of phase separation between the two phases present.

The Ce 3d XPS spectra for the catalysts are presented in Figure 11. Fine detail is hard to extract for the mechanochemically prepared sample due to high amounts of surface charging. causing the broad peak from 890–910 eV. However, a peak at 917 eV was present, and it is due to Ce^{4+}. This peak was present in all catalyst samples. With the exception of the carbonate mechanochemical catalyst, all the others contain a doublet at around 900 eV, indicative of Ce^{3+}. However, they were not as symmetrical as seen for the Na_2CO_3-prepared sample suggesting that not as much manganese incorporation into the lattice occurred for these other preparation techniques.

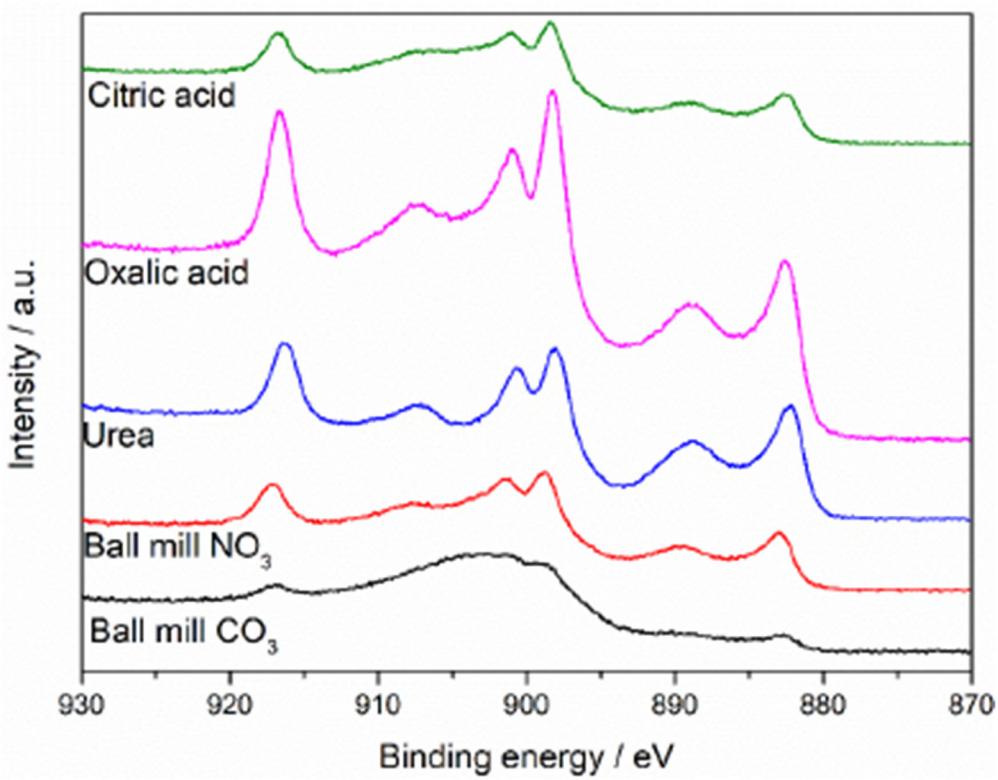

Figure 11. Ce 3d XPS spectra for $Ce_{0.25}Mn_{0.75}O_x$ catalysts.

The magnitude of splitting of the Mn 3s peaks can be seen in Table 4 (spectra in Figure S6). It shows that, like the Na_2CO_3 prepared catalyst, the mechanochemical catalysts had manganese in a 3+ oxidation state forming Mn_2O_3. The citric acid and oxalic acid samples had a smaller peak splitting indicating the presence of less catalytically active MnO_2.

Table 4. Magnitude of Mn 3s peak splitting determined from Mn 3s XPS spectra.

Sample	Magnitude of Mn 3s Peak Splitting/eV
Mechanochemical–carbonates	5.5
Mechanochemical–nitrates	5.7
Urea coprecipitation	-
Oxalic acid coprecipitation	5.2
Citric acid coprecipitation	4.9

3. Experimental

3.1. Catalyst Preparation

A set of ceria-manganese mixed metal oxide catalysts were prepared by coprecipitation using an auto-titration method (Metrohm Titrando, Runcorn, UK). The Ce:Mn ratios investigated were 100:0, 95:5, 90:10, 75:25, 50:50, 25:75, 0:100. Appropriate amounts of $Ce(NO_3)_3.6H_2O$ (Sigma-Aldrich, Gillingham, UK, 99%, 0.25 M) and $Mn(NO_3)_2.4H_2O$ (Sigma-Aldrich, Gillingham, UK, 99%, 0.25 M) solutions were added to a thermostatically controlled water-jacketed heated vessel and Na_2CO_3 solution (anhydrous, Sigma-Aldrich, Gillingham, UK, 1 M) was dosed at 3 mL min^{-1} at a constant pH of 9. The solution was aged at 60 °C for 2 h with the precipitate recovered and washed with 1 L of warm water. The sample was then dried for 16 h at 110 °C and calcined at 500 °C for 3 h under flowing air.

A $Ce_{0.25}Mn_{0.75}O_x$ sample was prepared by urea co-precipitation following methods described in Sellick et al. [36]. An appropriate amount of $(NH_4)_2Ce(NO_3)_6$ (Sigma-Aldrich, Gillingham, UK, 99%) and $Mn(NO_3)_2.4H_2O$ (Sigma-Aldrich, Gillingham, UK, 99%) were added to a round bottom flask containing 50 mL of deionised water. Urea (3.325 g, Sigma-Aldrich, Gillingham, UK, 99%) was added with the solution stirred under reflux for 24 h. The resulting precipitate was recovered, washed, and dried for 16 h at 110 °C. The sample was then calcined at 500 °C for 3 h under flowing air.

A $Ce_{0.25}Mn_{0.75}O_x$ sample was prepared by oxalic acid co-precipitation following methods described by Ishikawa et al. [54]. An appropriate amount of $Ce(NO_3)_3.6H_2O$ (Sigma-Aldrich, Gillingham, UK, 99%) and $Mn(NO_3)_2.4H_2O$ (Sigma-Aldrich, Gillingham, UK, 99%) were added to a beaker containing 200 mL ethanol. The mixture was stirred before oxalic acid (0.024 moles, Sigma-Aldrich, Gillingham, UK, 99%) was added. The solution was aged for 2 h at room temperature. The precipitate was filtered off and washed with 500 mL ethanol and dried in an oven at 110 C for 16 h. The material was then calcined at 500 °C for 3 h under flowing air.

A $Ce_{0.25}Mn_{0.75}O_x$ sample was prepared by citric acid co-precipitation following methods described by Trikalitis et al. [55]. An appropriate amount of $(NH_4)_2Ce(NO_3)_6$ (Sigma-Aldrich, Gillingham, UK, 99%) and $Mn(NO_3)_2.4H_2O$ (Sigma-Aldrich, Gillingham, UK, 99%) and citric acid (0.024 moles, Sigma-Aldrich, Gillingham, UK, >99.5%) were added to a round bottom flask containing 50 mL of deionised water and stirred at 90 °C for 30 min. The solution was then aged at 110 °C for 16 h with the resulting sample dried in an oven for 16 h at 110 °C. The solid was then placed in a ceramic crucible and heated in a muffle oven at 200 °C for 2 h. The sample was then calcined at 500 °C for 3 h under flowing air.

A $Ce_{0.25}Mn_{0.75}O_x$ sample was prepared mechanochemically using a planetary ball mill (Retsch PM100, Hope Valley, UK) with either $MnCO_3$ or $Mn(NO_3)_2.4H_2O$ used as the manganese precursor. An appropriate amount of $Ce_2(CO_3)_3$ (Sigma-Aldrich, Gillingham, UK, 99.9%) and $MnCO_3$ (Sigma-Aldrich, Gillingham, UK, 99%) or $Mn(NO_3)_2.4H_2O$ (Sigma-Aldrich, Gillingham, UK, 99%) were placed in the ball mill and ground for 4 h at 200 rpm. The resulting material was calcined at 500 °C under flowing air for 3 h.

3.2. Catalyst Testing

Catalyst performance testing was undertaken using gas-phase fixed bed microreactors (Carbolite Gero, Hope Valley, UK). Samples were secured between plugs of quartz wool in a 6 mm o.d. stainless steel reactor tube.

Propane oxidation was conducted at constant catalyst volume using a 50 mL min^{-1} flow of 5000 ppm propane in air with a gas hourly space velocity (GHSV) of 45,000 h^{-1}. The reaction was studied between 200 and 600 °C at 50 °C intervals and was controlled by a K-type thermocouple placed in the catalyst bed. The catalyst was allowed to stabilise at each reaction temperature and analysis repeated until three consistent sets of data were attained, ensuring that catalyst activity was measured at steady state. Online analysis was performed using gas chromatography (Agilent 7090B, Stockport, UK) with a thermal

conductivity detector (TCD) and flame ionization detector (FID). The TCD monitored concentrations of N_2 and O_2, and the FID analysed CO_2, CO, and hydrocarbon concentrations through use of a methanizer. Separation of the gasses was enabled by two columns: a Haysep Q (80–100 mesh, 1.8 m × 3.2 mm) and a MolSieve 13 X (80–100 mesh, 2 m × 3.2 mm).

Naphthalene oxidation was performed using a flow of 100 ppm naphthalene in He/O_2 at 50 mL min^{-1}. Naphthalene was sublimed in a furnace thermostatically controlled at 35 °C under a 40 mL min^{-1} flow of He, with O_2 (10 mL min^{-1}) added to the flow giving a total flow rate of 50 mL min^{-1}. The reaction was monitored between 100 and 250 °C at 25 °C intervals with the temperature controlled using a K-type thermocouple in the catalyst bed. Reactants and products were measured using online gas chromatography (Agilent 7090R, Stockport, UK) with Haysep Q (80–100 mesh, 3 m × 3.2 mm) and HP-5 (30 m × 0.32 mm × 0.25 μm) columns, with methanizer FID detectors. Catalyst performance was measured after suitable stabilisation time to attain steady state, this was confirmed by achieving three sets of consistent analysis data.

3.3. Catalyst Characterisation

Powder X-ray diffraction was performed using a Panalytical X'Pert (Malvern Panalytical, Malvern, UK) with a Cu X-ray source which operated at 40 mA and 40 kV. Phase identification was assisted by the ICDD standard database. Crystallite size was estimated by using the Scherrer equation where the line widths of four diffraction peaks were compared to a silicon standard.

Surface area analysis was determined using a Quantachrome Quadrasorb Evo Analyser (Quantachrome, Hook, UK). Samples were degassed at 250 °C under vacuum for 16 h before a 5-point N_2 adsorption isotherm was performed at −196 °C. The Braunauer–Emmett–Teller (BET) method was used to establish sample surface area.

Raman spectra were measured using a Renishaw inVia confocal Raman microscope (Renishaw, Gloucestershire, UK) with an argon ion visible green laser. The laser wavelength was 514 nm with spectra recorded in reflective mode using a charge couple device detector.

Temperature programmed reduction (TPR) was carried out using a Quantachrome ChemBET (Quantachrome, Hook, UK). Approximately 50 mg of sample was used during analysis. Catalysts were treated under a helium flow at 120 °C for an hour before a reduction profile was obtained under a flow of 10% H_2/Ar from room temperature to 900 °C. A temperature ramp of 15 C min^{-1} was used.

X-ray photoelectron spectroscopy (XPS) was performed using a Thermo Scientific K-Alpha+ spectrometer (Thermo Fisher Scientific, East Grinstead, UK) with an Al Kα monochromator operating at 72 W. Survey and high-resolution scans were recorded at pass energies of 150 eV and 40 eV, respectively, with scan step sizes of 1 and 0.1 eV. Combined fluxes of low-energy electrons and Ar ions were used to neutralise surface charging. Each spectrum was calibrated against the C (1s) peak at 284.8 eV. Data analysis was achieved using CasaXPS software v2.3.24 applying Schofield sensitivity factors and an energy dependence of −0.6, after removing the Shirley background.

Scanning electron microscopy (SEM) and electron dispersive X-ray spectroscopy (EDX) were performed using a Tescan MAIA3 FEG-SEM microscope (Tescan, Cambridge, UK) with an Oxford Instruments X-ray Max^N 80 (Oxford Instruments, Abingdon, UK) detector attachment.

4. Conclusions

Several ratios of ceria-manganese mixed metal oxides prepared by coprecipitation with Na_2CO_3 were investigated for the catalytic total oxidation of propane and naphthalene. All were active and activity increased as the proportion of manganese increased. This was ascribed to the increased incorporation of manganese into the ceria lattice. The $Ce_{0.25}Mn_{0.75}O_x$ catalyst was found to be the most active Ce:Mn ratio for both reactions. This

catalyst had phase separation of manganese substituted ceria along with highly active Mn_2O_3 phases that were not detected in the other catalysts. EDX and XPS analysis showed high levels of sodium present at the surface, suggesting an alternative preparation technique that could synthesise catalysts with greater performance.

This was tested by synthesising the most active $Ce_{0.25}Mn_{0.75}O_x$ using techniques that did not use a sodium precursor. The preparation method led to significant differences in both the characteristics and activities of the catalysts. In samples prepared mechanochemically from carbonate, and by urea, co-precipitation was more active for propane oxidation than the Na_2CO_3 precipitated catalyst due to increased phase separation giving distinct ceria and manganese oxide regions with smaller crystallite size. However, none of the non-sodium catalysts were more active for naphthalene oxidation, suggesting the presence of sodium does not influence this reaction as much as it does for total propane oxidation. Overall, very different catalysts were synthesised with properties ranging widely due to the synthesis method. This shows that the preparation technique should be carefully chosen when synthesising catalysts for a specific reaction.

Supplementary Materials: The following are available online at https://www.mdpi.com/article/10.3390/catal13010114/s1, Figure S1: Raman spectra of cerium-manganese mixed metal oxides prepared by sodium carbonate co-precipitation, Figure S2: SEM images of mixed metal oxides prepared by sodium carbonate co-precipitation, Figure S3: SEM-EDX images of mixed metal oxides prepared by sodium carbonate co-precipitation, Figure S4: SEM images of Ce0.25Mn0.75Ox prepared using different preparation techniques, Figure S5: SEM-EDX mapping of Ce0.25Mn0.75Ox prepared using different preparation techniques, Figure S6: Mn 2p XPS spectra of the Ce0.25Mn0.75Ox catalysts prepared by different methods, Table S1: Rate of reaction normalised to surface area for ceria-manganese mixed metal oxides prepared by sodium carbonate coprecipitation, Table S2: XPS derived surface elemental concentrations for ceria-manganese mixed metal oxide catalysts prepared by co-precipitation with sodium carbonate, Table S3: Rate of reaction normalised to surface area for Ce0.25Mn0.75Ox catalyst prepared by different techniques.

Author Contributions: Conceptualization, S.H.T.; Data curation, P.M.S.; Formal analysis, P.M.S. and L.A.B.; Investigation, S.H.T.; Writing—Review and editing, P.M.S., L.A.B. and S.H.T. All authors have read and agreed to the published version of the manuscript.

Funding: This research received no external funding.

Data Availability Statement: Data is contained within the article.

Acknowledgments The authors gratefully acknowledge the contribution of David Morgan for running the XPS experiments.

Conflicts of Interest: The authors declare no conflict of interest.

References

1. He, C.; Cheng, J.; Zhang, X.; Douthwaite, M.; Pattisson, S.; Hao, Z. Recent Advances in the Catalytic Oxidation of Volatile Organic Compounds: A Review Based on Pollutant Sorts and Sources. *Chem. Rev.* **2019**, *119*, 4471–4568.
2. Evuti, A. International Journal of Engineering Sciences A Synopsis on Biogenic and Anthropogenic Volatile Organic Compounds Emissions: Hazards and Control. *TI Int. J. Eng. Sci.* **2013**, *2*, 145–153.
3. Duan, J.; Tan, J.; Yang, L.; Wu, S.; Hao, J. Concentration, Sources and Ozone Formation Potential of Volatile Organic Compounds (VOCs) during Ozone Episode in Beijing. *Atmos. Res.* **2008**, *88*, 25–35. https://doi.org/10.1016/j.atmosres.2007.09.004.
4. Ryerson, T.B.; Trainer, M.; Holloway, J.S.; Parrish, D.D.; Huey, L.G.; Sueper, D.T.; Frost, G.J.; Donnelly, S.G.; Schauffler, S.; Atlas, E.L.; et al. Observations of Ozone Formation in Power Plant Plumes and Implications for Ozone Control Strategies. *Science* **2001**, *292*, 719–723. https://doi.org/10.1126/science.1058113.
5. Landrigan, P.J.; Fuller, R.; Acosta, N.J.R.; Adeyi, O.; Arnold, R.; Basu, N.; Baldé, A.B.; Bertollini, R.; Bose-O'Reilly, S.; Boufford, J.I.; et al. The Lancet Commission on Pollution and Health. *Lancet* **2018**, *391*, 462–512. https://doi.org/10.1016/S0140-6736(17)32345-0.
6. Scirè, S.; Liotta, L.F. Supported Gold Catalysts for the Total Oxidation of Volatile Organic Compounds. *Appl. Catal. B Environ.* **2012**, *125*, 222–246. https://doi.org/10.1016/j.apcatb.2012.05.047.
7. Guo, Y.; Wen, M.; Li, G.; An, T. Recent Advances in VOC Elimination by Catalytic Oxidation Technology onto Various Nanoparticles Catalysts: A Critical Review. *Appl. Catal. B Environ.* **2021**, *281*, 119447. https://doi.org/10.1016/j.apcatb.2020.119447.

8. Krishnamurthy, A.; Adebayo, B.; Gelles, T.; Rownaghi, A.; Rezaei, F. Abatement of Gaseous Volatile Organic Compounds: A Process Perspective. *Catal. Today* **2020**, *350*, 100–119. https://doi.org/10.1016/j.cattod.2019.05.069.
9. Yang, C.; Miao, G.; Pi, Y.; Xia, Q.; Wu, J.; Li, Z.; Xiao, J. Abatement of Various Types of VOCs by Adsorption/Catalytic Oxidation: A Review. *Chem. Eng. J.* **2019**, *370*, 1128–1153. https://doi.org/10.1016/j.cej.2019.03.232.
10. Taylor, M.N.; Zhou, W.; Garcia, T.; Solsona, B.; Carley, A.F.; Kiely, C.J.; Taylor, S.H. Synergy between Tungsten and Palladium Supported on Titania for the Catalytic Total Oxidation of Propane. *J. Catal.* **2012**, *285*, 103–114. https://doi.org/10.1016/j.jcat.2011.09.019.
11. Tichenor, B.A.; Palazzolo, M.A. Destruction of Volatile Organic Compounds via Catalytic Incineration. *Environ. Prog.* **1987**, *6*, 172–176. https://doi.org/10.1002/ep.670060328.
12. Enterkin, J.A.; Setthapun, W.; Elam, J.W.; Christensen, S.T.; Rabuffetti, F.A.; Marks, L.D.; Stair, P.C.; Poeppelmeier, K.R.; Marshall, C.L. Propane Oxidation over Pt/SrTiO3 Nanocuboids. *ACS Catal.* **2011**, *1*, 629–635. https://doi.org/10.1021/cs200092c.
13. García, T.; Solsona, B.; Taylor, S.H. Naphthalene Total Oxidation over Metal Oxide Catalysts. *Appl. Catal. B Environ.* **2006**, *66*, 92–99. https://doi.org/10.1016/j.apcatb.2006.03.003.
14. Sharma, R.K.; Zhou, B.; Tong, S.; Chuang, K.T. Catalytic Destruction of Volatile Organic Compounds Using Supported Platinum and Palladium Hydrophobic Catalysts. *Ind. Eng. Chem. Res.* **1995**, *34*, 4310–4317. https://doi.org/10.1021/ie00039a022.
15. Aggett, K.; Davies, T.E.; Morgan, D.J.; Hewes, D.; Taylor, S.H. The Influence of Precursor on the Preparation of CeO_2 Catalysts for the Total Oxidation of the Volatile Organic Compound Propane. *Catalysts* **2021**, *11*, 1461. https://doi.org/10.3390/catal11121461.
16. Montini, T.; Melchionna, M.; Monai, M.; Fornasiero, P. Fundamentals and Catalytic Applications of CeO_2-Based Materials. *Chem. Rev.* **2016**, *116*, 5987–6041. https://doi.org/10.1021/acs.chemrev.5b00603.
17. Garcia, T.; Solsona, B.; Taylor, S.H. Nano-Crystalline Ceria Catalysts for the Abatement of Polycyclic Aromatic Hydrocarbons. *Catal. Lett.* **2005**, *105*, 183–189. https://doi.org/10.1007/s10562-005-8689-2.
18. Setiabudi, A.; Chen, J.; Mul, G.; Makkee, M.; Moulijn, J.A. CeO2 Catalysed Soot Oxidation: The Role of Active Oxygen to Accelerate the Oxidation Conversion. *Appl. Catal. B Environ.* **2004**, *51*, 9–19. https://doi.org/10.1016/j.apcatb.2004.01.005.
19. Zheng, X.; Li, Y.; Zhang, L.; Shen, L.; Xiao, Y.; Zhang, Y.; Au, C.; Jiang, L. Insight into the Effect of Morphology on Catalytic Performance of Porous CeO_2 Nanocrystals for H2S Selective Oxidation. *Appl. Catal. B Environ.* **2019**, *252*, 98–110. https://doi.org/10.1016/j.apcatb.2019.04.014.
20. Shah, P.M.; Day, A.N.; Davies, T.E.; Morgan, D.J.; Taylor, S.H. Mechanochemical Preparation of Ceria-Zirconia Catalysts for the Total Oxidation of Propane and Naphthalene Volatile Organic Compounds. *Appl. Catal. B Environ.* **2019**, *253*, 331–340. https://doi.org/10.1016/j.apcatb.2019.04.061.
21. Shah, P.M.; Burnett, J.W.H.; Morgan, D.J.; Davies, T.E.; Taylor, S.H. Ceria–Zirconia Mixed Metal Oxides Prepared via Mechanochemical Grinding of Carbonates for the Total Oxidation of Propane and Naphthalene. *Catalysts* **2019**, *9*, 475. https://doi.org/10.3390/catal9050475.
22. Feng, Q.; Kanoh, H.; Ooi, K. Manganese Oxide Porous Crystals. *J. Mater. Chem.* **1999**, *9*, 319–333. https://doi.org/10.1039/A805369C.
23. Garcia, T.; Sellick, D.; Varela, F.; Vázquez, I.; Dejoz, A.; Agouram, S.; Taylor, S.H.; Solsona, B. Total Oxidation of Naphthalene Using Bulk Manganese Oxide Catalysts. *Appl. Catal. A Gen.* **2013**, *450*, 169–177. https://doi.org/10.1016/j.apcata.2012.10.029.
24. Qi, G.; Li, W. NO Oxidation to NO_2 over Manganese-Cerium Mixed Oxides. *Catal. Today* **2015**, *258*, 205–213. https://doi.org/10.1016/j.cattod.2015.03.020.
25. Liang, Y.; Huang, Y.; Zhang, H.; Lan, L.; Zhao, M.; Gong, M.; Chen, Y.; Wang, J. Interactional Effect of Cerium and Manganese on NO Catalytic Oxidation. *Environ. Sci. Pollut. Res.* **2017**, *24*, 9314–9324. https://doi.org/10.1007/s11356-017-8645-x.
26. Venkataswamy, P.; Rao, K.N.; Jampaiah, D.; Reddy, B.M. Nanostructured Manganese Doped Ceria Solid Solutions for CO Oxidation at Lower Temperatures. *Appl. Catal. B Environ.* **2015**, *162*, 122–132. https://doi.org/10.1016/j.apcatb.2014.06.038.
27. Liu, X.; Lu, J.; Qian, K.; Huang, W.; Luo, M. A Comparative Study of Formaldehyde and Carbon Monoxide Complete Oxidation on MnOx-CeO_2 Catalysts. *J. Rare Earths* **2009**, *27*, 418–424. https://doi.org/10.1016/S1002-0721(08)60263-X.
28. Li, H.; Qi, G.; Tana; Zhang, X.; Huang, X.; Li, W.; Shen, W. Low-Temperature Oxidation of Ethanol over a $Mn_{0.6}Ce0.4O_2$ Mixed Oxide. *Appl. Catal. B Environ.* **2011**, *103*, 54–61. https://doi.org/10.1016/j.apcatb.2011.01.008.
29. Delimaris, D.; Ioannides, T. Intrinsic Activity of MnOx-CeO_2 Catalysts in Ethanol Oxidation. *Catalysts* **2017**, *7*, 339. https://doi.org/10.3390/catal7110339.
30. Chen, H.; Sayari, A.; Adnot, A.; Larachi, F. Composition–Activity Effects of Mn–Ce–O Composites on Phenol Catalytic Wet Oxidation. *Appl. Catal. B Environ.* **2001**, *32*, 195–204. https://doi.org/10.1016/S0926-3373(01)00136-9.
31. Arena, F.; Negro, J.; Parmaliana, A.; Spadaro, L.; Trunfio, G. Improved MnCeOx Systems for the Catalytic Wet Oxidation (CWO) of Phenol in Wastewater Streams. *Ind. Eng. Chem. Res.* **2007**, *46*, 6724–6731. https://doi.org/10.1021/ie0701118.
32. Chen, J.; Chen, X.; Chen, X.; Xu, W.; Xu, Z.; Jia, H.; Chen, J. Homogeneous Introduction of CeOy into MnOx-Based Catalyst for Oxidation of Aromatic VOCs. *Appl. Catal. B Environ.* **2018**, *224*, 825–835. https://doi.org/10.1016/j.apcatb.2017.11.036.
33. Matějová, L.; Topka, P.; Jirátová, K.; Šolcová, O. Total Oxidation of Model Volatile Organic Compounds over Some Commercial Catalysts. *Appl. Catal. A Gen.* **2012**, *443–444*, 40–49. https://doi.org/10.1016/j.apcata.2012.07.018.
34. Xu, Y.; Mofarah, S.; Mehmood, R.; Cazorla, C.; Koshy, P.; Sorrell, C. Design Strategies for Ceria Nanomaterials: Untangling Key Mechanistic Concepts. *Mater. Horiz.* **2021**, *8*, 102–123. https://doi.org/10.1039/D0MH00654H.

35. Thakur, N.; Manna, P.; Das, J. Synthesis and Biomedical Applications of Nanoceria, a Redox Active Nanoparticle. *J. Nanobiotechnology* **2019**, *17*, 84. https://doi.org/10.1186/s12951-019-0516-9.
36. Sellick, D.R.; Aranda, A.; García, T.; López, J.M.; Solsona, B.; Mastral, A.M.; Morgan, D.J.; Carley, A.F.; Taylor, S.H. Influence of the Preparation Method on the Activity of Ceria Zirconia Mixed Oxides for Naphthalene Total Oxidation. *Appl. Catal. B Environ.* **2013**, *132–133*, 98–106. https://doi.org/10.1016/j.apcatb.2012.11.036.
37. Ntainjua, E.N.; Davies, T.E.; Garcia, T.; Solsona, B.; Taylor, S.H. The Influence of Platinum Addition on Nano-Crystalline Ceria Catalysts for the Total Oxidation of Naphthalene a Model Polycyclic Aromatic Hydrocarbon. *Catal. Lett.* **2011**, *141*, 1732–1738. https://doi.org/10.1007/s10562-011-0710-3.
38. Smith, L.R.; Sainna, M.A.; Douthwaite, M.; Davies, T.E.; Dummer, N.F.; Willock, D.J.; Knight, D.W.; Catlow, C.R.A.; Taylor, S.H.; Hutchings, G.J. Gas Phase Glycerol Valorization over Ceria Nanostructures with Well-Defined Morphologies. *ACS Catal.* **2021**, *11*, 4893–4907. https://doi.org/10.1021/acscatal.0c05606.
39. Ren, T.-Z.; Xu, P.-B.; Deng, Q.-F.; Yuan, Z.-Y. Mesoporous Ce1−xMnxO_2 Mixed Oxides with CuO Loading for the Catalytic Total Oxidation of Propane. *Reac. Kinet. Mech. Cat.* **2013**, *110*, 405–420. https://doi.org/10.1007/s11144-013-0603-0.
40. Zhan, S.; Zhu, D.; Qiu, M.; Yu, H.; Li, Y. Highly Efficient Removal of NO with Ordered Mesoporous Manganese Oxide at Low Temperature. *RSC Advances* **2015**, *5*, 29353–29361. https://doi.org/10.1039/C4RA17300G.
41. Augustin, M.; Fenske, D.; Bardenhagen, I.; Westphal, A.; Knipper, M.; Plaggenborg, T.; Kolny-Olesiak, J.; Parisi, J. Manganese Oxide Phases and Morphologies: A Study on Calcination Temperature and Atmospheric Dependence. *Beilstein. J. Nanotechnol.* **2015**, *6*, 47–59. https://doi.org/10.3762/bjnano.6.6.
42. Jampaiah, D.; Venkataswamy, P.; Tur, K.M.; Ippolito, S.J.; Bhargava, S.K.; Reddy, B.M. Effect of MnOx Loading on Structural, Surface, and Catalytic Properties of CeO_2-MnOx Mixed Oxides Prepared by Sol-Gel Method. *Z. Für Anorg. Und Allg. Chem.* **2015**, *641*, 1141–1149. https://doi.org/10.1002/zaac.201400615.
43. Liu, L.; Shi, J.; Zhang, X.; Liu, J. Flower-Like Mn-Doped CeO_2 Microstructures: Synthesis, Characterizations, and Catalytic Properties. *J. Chem.* **2015**, *2015*, e254750. https://doi.org/10.1155/2015/254750.
44. Spanier, J.E.; Robinson, R.D.; Zhang, F.; Chan, S.-W.; Herman, I.P. Size-Dependent Properties of CeO2 Nanoparticles as Studied by Raman Scattering. *Phys. Rev. B* **2001**, *64*, 245407. https://doi.org/10.1103/PhysRevB.64.245407.
45. Huang, H.; Liu, J.; Sun, P.; Ye, S.; Liu, B. Effects of Mn-Doped Ceria Oxygen-Storage Material on Oxidation Activity of Diesel Soot. *RSC Adv.* **2017**, *7*, 7406–7412. https://doi.org/10.1039/C6RA27007G.
46. Wang, H.; Chen, X.; Gao, S.; Wu, Z.; Liu, Y.; Weng, X. Deactivation Mechanism of Ce/TiO_2 Selective Catalytic Reduction Catalysts by the Loading of Sodium and Calcium Salts. *Catal. Sci. Technol.* **2013**, *3*, 715–722. https://doi.org/10.1039/C2CY20568H.
47. Mirzaei, A.A.; Shaterian, H.R.; Joyner, R.W.; Stockenhuber, M.; Taylor, S.H.; Hutchings, G.J. Ambient Temperature Carbon Monoxide Oxidation Using Copper Manganese Oxide Catalysts: Effect of Residual Na+ Acting as Catalyst Poison. *Catal. Commun.* **2003**, *4*, 17–20. https://doi.org/10.1016/S1566-7367(02)00231-5.
48. Junta, J.L.; Hochella, M.F. Manganese (II) Oxidation at Mineral Surfaces: A Microscopic and Spectroscopic Study. *Geochim. Et Cosmochim. Acta* **1994**, *58*, 4985–4999. https://doi.org/10.1016/0016-7037(94)90226-7.
49. Tang, W.; Wu, X.; Liu, G.; Li, S.; Li, D.; Li, W.; Chen, Y. Preparation of Hierarchical Layer-Stacking Mn-Ce Composite Oxide for Catalytic Total Oxidation of VOCs. *J. Rare Earths* **2015**, *33*, 62–69. https://doi.org/10.1016/S1002-0721(14)60384-7.
50. Du, J.; Qu, Z.; Dong, C.; Song, L.; Qin, Y.; Huang, N. Low-Temperature Abatement of Toluene over Mn-Ce Oxides Catalysts Synthesized by a Modified Hydrothermal Approach. *Appl. Surf. Sci.* **2018**, *433*, 1025–1035. https://doi.org/10.1016/j.apsusc.2017.10.116.
51. Stobbe, E.R.; de Boer, B.A.; Geus, J.W. The Reduction and Oxidation Behaviour of Manganese Oxides. *Catal. Today* **1999**, *47*, 161–167. https://doi.org/10.1016/S0920-5861(98)00296-X.
52. Rudisill, S.G.; Hein, N.M.; Terzic, D.; Stein, A. Controlling Microstructural Evolution in Pechini Gels through the Interplay between Precursor Complexation, Step-Growth Polymerization, and Template Confinement. *Chem. Mater.* **2013**, *25*, 745–753. https://doi.org/10.1021/cm303761z.
53. Winck, L.B.; de Almeida Ferreira, J.L.; Martinez, J.M.G.; Araujo, J.A.; Rodrigues, A.C.M.; da Silva, C.R.M. Synthesis, Sintering and Characterization of Ceria-Based Solid Electrolytes Codoped with Samaria and Gadolinium Using the Pechini Method. *Ceram. Int.* **2017**, *43*, 16408–16415. https://doi.org/10.1016/j.ceramint.2017.09.017.
54. Ishikawa, S.; Jones, D.R.; Iqbal, S.; Reece, C.; Morgan, D.J.; Willock, D.J.; Miedziak, P.J.; Bartley, J.K.; Edwards, J.K.; Murayama, T.; et al. Identification of the Catalytically Active Component of Cu–Zr–O Catalyst for the Hydrogenation of Levulinic Acid to γ-Valerolactone. *Green Chem.* **2017**, *19*, 225–236. https://doi.org/10.1039/C6GC02598F.
55. Trikalitis, P.N.; Pomonis, P.J. Catalytic Activity and Selectivity of Perovskites La1−xSrxV1−x3+Vx4+O3 for the Transformation of Isopropanol. *Appl. Catal. A Gen.* **1995**, *131*, 309–322. https://doi.org/10.1016/0926-860X(95)00121-2.